

Article

New Crystal Forms for Biologically Active Compounds. Part 1: Noncovalent Interactions in Adducts of Nevirapine with XB Donors

Mariya A. Kryukova, Alexander V. Sapegin, Alexander S. Novikov , Mikhail Krasavin and Daniil M. Ivanov * 

Saint Petersburg State University, Saint Petersburg 199034, Russia; Mary_Kryukova@mail.ru (M.A.K.); sapegin_yar@mail.ru (A.V.S.); ja2-88@mail.ru (A.S.N.); krasavintm@gmail.com (M.K.)

* Correspondence: dan15101992@gmail.com

Received: 12 January 2019; Accepted: 29 January 2019; Published: 30 January 2019



Abstract: Stabilization of specific crystal polymorphs of an active pharmaceutical ingredient is crucial for preventing uncontrollable interconversion of various crystalline forms, which affects physicochemical properties as well as physiological activity. Co-crystallization with various excipients is an emerging productive way of achieving such stabilization in the solid state. In this work, we identified an opportunity for co-crystallization of antiviral drug nevirapine (NVP) with a classical XB donor, 1,2,4,5-tetrafluoro-3,6-diiodobenzene (1,4-FIB), as well as 1,3-diiodobenzene (1,3-DIB), which has been seldom employed as an XB donor to date. In the X-ray structures of NVP·1,4-FIB and NVP·1,3-DIB co-crystals, different hydrogen and halogen bonding modes were detected and further investigated via DFT calculations as well as topological analysis of the electron density distribution within the framework of the QTAIM method at the M06/DZP-DKH level of theory. Estimated energies of these supramolecular contacts vary from 0.6 to 5.7 kcal/mol.

Keywords: nevirapine; crystal engineering; noncovalent interactions; halogen bonding; hydrogen bonding; DFT; QTAIM

1. Introduction

Important physicochemical properties of active pharmaceutical ingredients (APIs) such as melting point, rate of dissolution, hygroscopicity, as well as thermal, mechanical and even chemical properties can vary significantly depending on the particular solid form [1]. Existence of several polymorphic states can impede the solubility, stability, bioavailability and, as a result, the desired physiological activity of the drug. Therefore, controlling which form an API in question exists in, before it is made into an approved dosage form, is of critical importance [2]. Currently, 85% of known APIs exhibit (pseudo)polymorphism and 50% of APIs can exist in multiple forms [3]. Hence, the importance of developing reliable approaches to stabilizing a particular crystal form of an API cannot be overestimated. Ideally, a desired polymorph should be stabilized to such an extent that it becomes thermodynamically stable, is not affected by humidity levels (i.e., it does not form hydrates in humid environments) and, in general, acts as a monomorphic compound [4]. Judicious engineering of co-crystals (i.e., crystalline forms that consist of two or more components that are solid at room temperature) has attracted growing attention as a productive means of stabilizing an API in a specific solid form [5]. The development of an optimal, stable co-crystal entails elements of discovery and rational design and, therefore, carries aspects of utility, novelty and non-obviousness which are critical criteria for intellectual property protection [6]. This makes the process of co-crystal design and engineering an advantageous process in itself, potentially leading to excipients (non-API components of

the solid form) which can themselves be protected by a patent [7]. Moreover, engineering of completely novel crystal forms for an API with suboptimal physicochemical characteristics can lead to a novel solid form of a drug which is characterized by improved aqueous solubility and bioavailability [8].

The main principle of crystal engineering has been the ‘exploitation of noncovalent interactions between molecular or ionic components for the rational design of solid-state structures that might exhibit interesting electrical, magnetic, and optical properties’ [9]. Thus, co-crystallization has prominently emerged as a tool to generate multiple solid forms for a given API with an aim to select the most suitable ones [7,10–12]. Candidate co-crystals, in turn, can be obtained by crystallization from a solution [13–15] or by mechanochemical means [16–18].

To a prevailing degree, however, when noncovalent interactions are concerned, hydrogen bonding (HB) [19] is implied [20]. Considering that over the last decade, the halogen bond (XB) [21] has emerged as an effective tool for crystal engineering [22–29] and designing supramolecular constructs [30–32], it is surprising that literature reports on the utility of XB in engineering new API crystal forms has been relatively scarce [20,33–36]. Our recent engagement in crystal engineering based on XB in metal complexes [37–45] prompted us to consider exploring new opportunities for filling the above void and applying the XB approach towards identifying novel API crystal forms. We screened a number of important APIs for the formation of co-crystals with known potential as well as recently synthesized [46] donors of halogen bonds. One of the APIs employed in our program was the known antiviral drug nevirapine (NVP, IUPAC name 11-cyclopropyl-4-methyl-5,11-dihydro-6H-dipyrido[3,2-b:2',3'-e][1,4]diazepin-6-one), which acts as non-nucleoside reverse transcriptase inhibitor (NNRTI) and is used for treatment of HIV-1 infection and AIDS [47,48]. In addition to antiviral activity, it has been reported to bind to CYP3A4 and CYP2B6 cytochromes [49] and to display some anticancer activity [50–52]. Various crystal structures of NVP have been described [53–60]. In the majority of these structures, the NVP molecule acts as an HB donor (via the N–H motif) and an HB acceptor (via the carbonyl O and pyridine N atoms).

We performed a comprehensive analysis of ten XRD structures of NVP solvates, two structures of unassociated NVP, and six structures of NVP adducts with carboxylic acids, saccharine and polycaprolactone using the Olex2 program. This analysis revealed that (i) the O carbonyl atom is the nucleophilic center for 51 noncovalent interactions including HBs and $\text{lp}(\text{O})\cdots\pi(\text{C})$ interactions; and (ii) the amide H atom is the electrophilic center for 23 examples of HBs. Other peripheral atoms are also involved in both HBs and $\text{lp}(\text{O})\cdots\pi(\text{C})$ interactions (Figure 1). Many of these contacts, especially the $\text{C}-\text{H}\cdots\text{X}$ ($\text{X} = \text{N}, \text{O}$) HBs, were not discussed or were simply overlooked in the corresponding reports, although they are real HBs in accordance with the IUPAC definition for HBs [19].

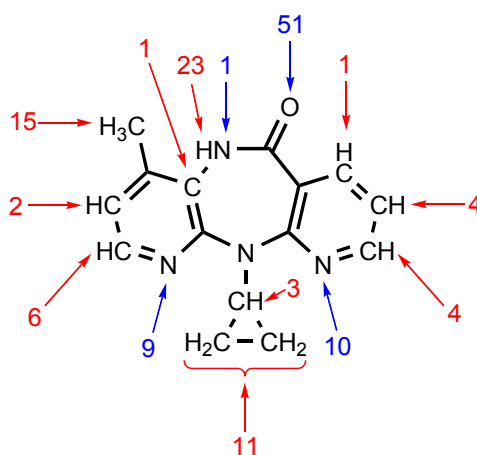


Figure 1. Statistical analysis results for the crystal structures containing nevirapine. Blue arrows highlight atoms that act as nucleophilic components of noncovalent interactions, while those acting as electrophilic components are marked by red arrows. Only the interactions of nondisordered fragments were taken into account, while π -stacking interactions were not.

Previously, we have already attempted [61] to involve NVP in co-crystallization with molecular iodine as an XB donor. Contrary to our expectations at the time, instead of a co-crystal, we obtained an intriguing salt form, nevirapinium pentaiodide hydrate, which was investigated by crystallography to reveal the presence of numerous HBs and an unusual $I_4-I \cdots O=C$ interionic XB. In continuation of these efforts, NVP was co-crystallized with 1,2,4,5-tetrafluoro-3,6-diiodobenzene (1,4-FIB), an XB donor that has already been employed in the co-crystal formation for such biologically active compounds as nicotine [62], pyrazinamide, lidocaine and pentoxifylline [20]. Additionally, we used 1,3-diiodobenzene (1,3-DIB), a rarely employed [63] XB donor. To our delight, both attempts resulted in the formation of nevirapine co-crystals with these XB donors. Herein, we present the results of these studies.

2. Experimental Section

2.1. Materials

Nevirapine, 1,2,4,5-tetrafluoro-3,6-diiodobenzene, 1,3-diiodobenzene and MeOH were obtained from commercial source and used as received.

2.2. X-ray Structure Determination

A crystal of NVP·1,3-DIB was measured on a SuperNova, Dual, Cu at zero, Atlas diffractometer at 100 K using monochromated MoK α ($\lambda = 0.7107$) radiation. A crystal of NVP·1,3-DIB was measured on an Xcalibur, Eos diffractometer at 100 K using monochromated MoK α ($\lambda = 0.7107$) radiation. The structures have been solved by the direct methods by means of the SHELX program [64] incorporated into the Olex2 program package [65]. For crystallographic data and refinement parameters, see Supplementary Material (Table S2). The carbon-bound H atoms were placed in calculated positions and were included in the refinement in the 'riding' model approximation, with $U_{iso}(H)$ set to $1.5U_{eq}(C)$ and C–H 0.98 Å for CH₃ groups, with $U_{iso}(H)$ set to $1.2U_{eq}(C)$ and C–H 0.99 Å for CH₂ groups and with $U_{iso}(H)$ set to $1.2U_{eq}(C)$, C–H 0.95 Å for CH groups. Empirical absorption correction was applied in the CrysAlisPro [66] program complex using spherical harmonics, and implemented in the SCALE3 ABSPACK scaling algorithm. Supplementary crystallographic data for this paper have been deposited at the Cambridge Crystallographic Data Centre (CCDC 1882105 and 1882106) and can be obtained free of charge via www.ccdc.cam.ac.uk/data_request/cif.

2.3. Computational Details

The single-point calculations based on the experimental X-ray geometries of NVP·1,4-FIB and NVP·1,3-DIB have been carried out at the DFT level of theory using the M06 functional [67] with the help of the Gaussian-09 [68] program package. The Douglas–Kroll–Hess 2nd-order scalar relativistic calculations requested relativistic core Hamiltonian were carried out using the DZP-DKH basis sets [69–72] for all atoms. The topological analysis of the electron density distribution with the help of the atoms in molecules (QTAIM) method developed by Bader [73] has been performed by using the Multiwfn program [74]. The Wiberg bond indices were computed by using the natural bond orbital (NBO) partitioning scheme [75]. The Cartesian atomic coordinates of model supramolecular clusters (NVP)₄·(1,4-FIB)₃ and (NVP)₃·(1,3-DIB)₃ are presented in Supporting Information, Table S3.

3. Results and Discussion

3.1. Halogen Bonding in NVP·1,4-FIB and NVP·1,3-DIB

Slow evaporation of MeOH solutions of NVP containing an equimolar amount of either 1,4-FIB or 1,3-DIB at room temperature gave co-crystals NVP·1,4-FIB and NVP·1,3-DIB, respectively. The results of the XRD study indicated that both adducts contained the C–I \cdots N XBs (Figure 2), numerous HBs as well as a number of other interactions. DFT calculations and topological analysis of the electron density distribution within the framework of the QTAIM method confirmed the noncovalent nature of

these contacts and allowed evaluation of their energies (0.6–5.7 kcal/mol) (for details see theoretical study section).

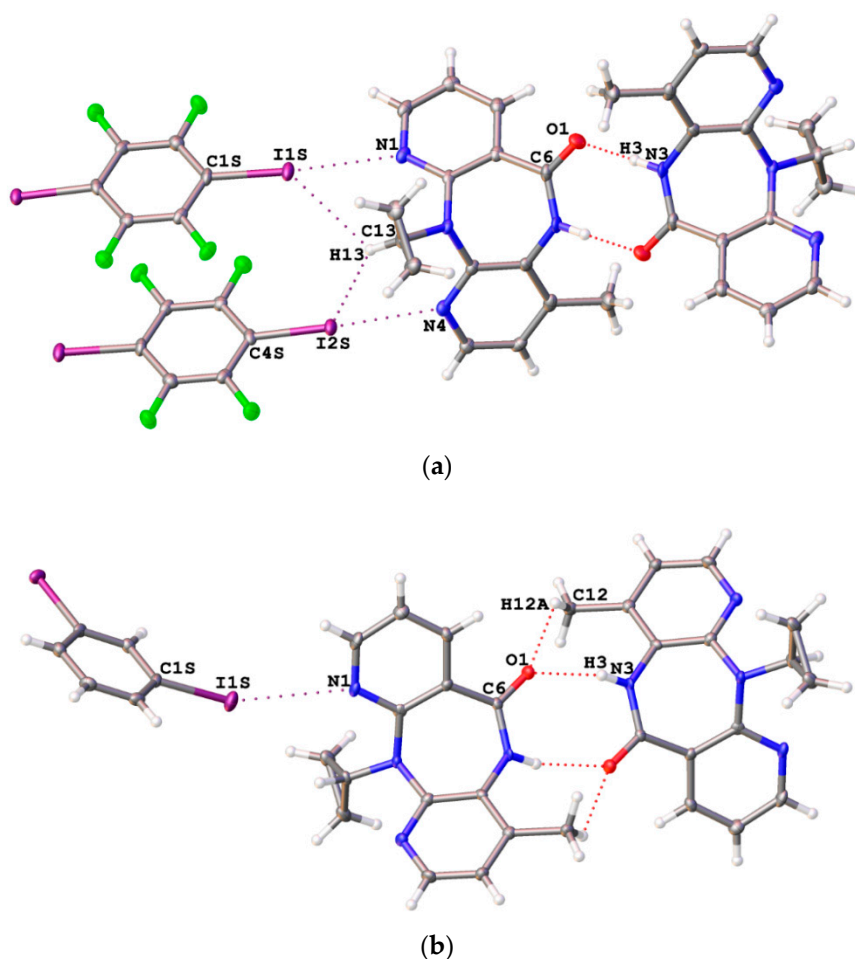


Figure 2. The important noncovalent interactions in NVP·1,4-FIB (a) and NVP·1,3-DIB (b) co-crystals obtained in this work.

In both adducts, one or both of the pyridine nitrogen atoms of nevirapine molecule were found to be involved in XBs as nucleophiles. In NVP·1,4-FIB, both pyridine nitrogen atoms form the C–I···N XBs with comparable geometric parameters (Table 1). Analysis of the data in CCDC related to C–I···N XBs between 1,4-FIB and various pyridine rings revealed that the shortest *p*-I–C₆F₄–I···N(pyridine) XB had been documented for an adduct of 1,4-FIB with 4-(dimethylamino)pyridine ($d(\text{I} \cdots \text{N}) = 2.6672(18)$ Å) [76] whereas the longest *p*-I–C₆F₄–I···N(pyridine) XB had been observed in a 1,4-FIB adduct with pyridine-2-thioamide ($d(\text{I} \cdots \text{N}) = 3.215(4)$ Å) [77]. Thus, the C–I···N XB lengths found in NVP·1,4-FIB (2.988(4) and 2.973(4) Å) fall within this range and can be regarded as rather common for the XBs between 1,4-FIB and a pyridine ring.

In the NVP·1,3-DIB co-crystal, only one nitrogen atom (that of the unsubstituted pyridine ring) forms a C–I···N XB (Table 1). To the best of our knowledge, this structure represents the second example of a supramolecular assembly where 1,3-DIB acts as XB donor. Previously, Uekusa et al. [63] reported the adduct of 1,3-DIB with *N*-(4-bromosalicylidene)-3-aminopyridine, demonstrating the C–I···N XBs (3.081(3) Å). It should be noted that isomeric 1,4-diiodobenzene (1,4-DIB) is a well-known participant in the C–I···N XBs. In most cases involving 1,4-DIB, the lengths of such contacts are in the range 2.928(4)–3.076(11) Å [23,78–81]. Noticeably larger lengths (3.313(3)–3.462(2) Å and 3.239(3) Å, respectively) were encountered in the case of bifurcate C–I···(N,N) contacts [82] as well as for

C–I...N≡C–R XB involving much less nucleophilic N_{sp} atoms [79]. Thus, the relatively long XB in the NVP·1,3-DIB co-crystal (3.231(3) Å) can be rationalized by steric rather than electronic effects.

Table 1. Parameters of the C–I...N XBs in the co-crystals obtained in this work.

Structure	C–I...N	<i>d</i> (I...N), Å	R _{IN} ²	∠(C–I...N), °	E _{int} ³	E _{int} ⁴
NVP·1,3-DIB	C1S–I1S...N1	3.231(3)	0.92	156.09(11)	2.5	2.4
NVP·1,4-FIB	C1S–I1S...N1	2.988(4)	0.85	174.33(10)	4.4	3.8
	C2S–I2S...N4	2.973(4)	0.84	175.88(13)	4.4	4.0
	Comparison ¹	3.53	1.00	180		

¹ Comparison is the vdW radii sum [83] for distances and classic XB angle. ² R_{IN} = *d*(I...N)/(R_{vdW}(I) + R_{vdW}(N)).

³ E_{int} = −V(r)/2 [84]. ⁴ E_{int} = 0.429G(r) [85].

3.2. Hydrogen Bonding in the NVP·1,4-FIB and NVP·1,3-DIB Co-Crystals

Dimerization of nevirapine molecules upon the N–H...O=C HB formation was evident in both structures (Figure 2). Almost the same supramolecular features can be found in NVP (PABHIJ [53] and PABHIJ01 [58]) crystals as well as in numerous crystals of nevirapine solvates (GIRWUA [54], KACPAH [55], OKETII [57], TISJEL [59], TISJEL01, YIVQIE, YIVQOK, YIVQUQ [58]) and adducts (LATQOO, LATQUU [56], ZEYSAA [60]). Only in co-crystals with relatively strong HB donors (H₂O, TISJAH [59] and TISJAH01 [58]; *cis*-HO₂C(CH=CH)CO₂H, LATQII; HO₂C(CH₂)₃CO₂H, LATQEE; HO₂C(CHOH)₂CO₂H, LATRAB [56]) is said dimerization absent because at least the C=O nevirapine functionality is involved in O–H...O=C HBs.

NVP·1,3-DIB also contains weaker C–H...O=C HBs supporting the N–H...O=C HBs (Figure 2), the C–H...N hydrogen bonding between NVP molecules, and the C–H...I interactions between 1,3-DIB molecules.

Notably, NVP·1,4-FIB demonstrated weak C–H...O and C–H...N interactions between NVP molecules, and the numerous C–H...F and C–H...I HBs between NVP and 1,4-FIB molecules. The latter interactions are interesting because the same C–H moiety in the cyclopropyl group is involved in both C–H...I interactions (Figure 2). Note that the simultaneous formation of HBs and XBs with the I atoms in 1,4-FIB was previously reported by us [42]. The geometrical parameters of HBs are represented in Table S1.

3.3. Theoretical Study of Different Noncovalent Interactions in NVP·1,4-FIB and NVP·1,3-DIB

Inspection of the crystallographic data suggests the presence of different noncovalent interactions responsible for the formation of a supramolecular structure of NVP·1,4-FIB and NVP·1,3-DIB. In light of this, in addition to structural analysis, a detailed computational study was undertaken. In order to confirm or disprove the hypothesis on the existence of these supramolecular contacts and quantify their energies from a theoretical standpoint, we carried out DFT calculations and performed topological analysis of the electron density distribution within the framework of Bader's theory (QTAIM method) [73] for the (NVP)₄·(1,4-FIB)₃ and (NVP)₃·(1,3-DIB)₃ model supramolecular cluster (Supporting Information, Table S3). We have already used a similar approach to study noncovalent interactions (e.g., hydrogen, halogen and chalcogen bonding, metallophilic interactions, stacking) in various organic, organometallic and coordination compounds [42–44,86–89]. The results of these calculations are summarized in Table 2. The contour line diagrams of the Laplacian distribution ∇²ρ(r), bond paths, and selected zero-flux surfaces for (NVP)₄·(1,4-FIB)₃ and (NVP)₃·(1,3-DIB)₃, are shown in Figure 3. To visualize the noncovalent interactions studied, we carried out reduced density gradient (RDG) analysis [90] and plotted RDG isosurfaces for (NVP)₄·(1,4-FIB)₃ and (NVP)₃·(1,3-DIB)₃ (Figure 3).

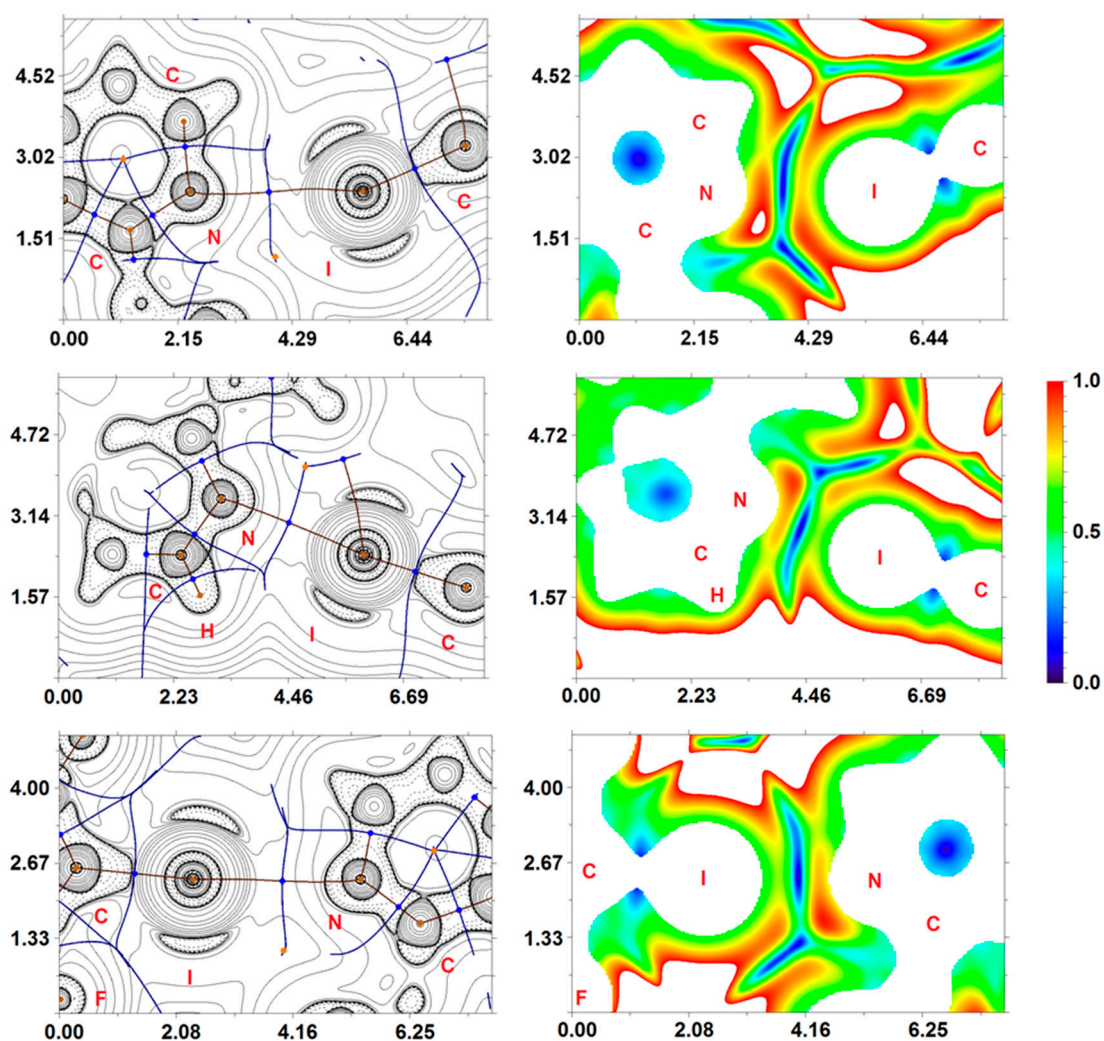


Figure 3. Contour line diagrams of the Laplacian distribution $\nabla^2\rho(\mathbf{r})$, bond paths and selected zero-flux surfaces (left), and RDG isosurfaces (right) referring to the C–I···N XBs in $(\text{NVP})_3\cdot(1,3\text{-DIB})_3$ (upper) and $(\text{NVP})_4\cdot(1,4\text{-FIB})_3$ (middle and lower). Bond critical points (3, -1) are shown in blue, nuclear critical points (3, -3) in pale brown, ring critical points (3, $+1$) in orange. Length units—Å, RDG isosurface values are given in a.u.

The QTAIM analysis of $(\text{NVP})_4\cdot(1,4\text{-FIB})_3$ and $(\text{NVP})_3\cdot(1,3\text{-DIB})_3$ demonstrated the presence of appropriate bond critical points (3, -1) (BCPs) for all noncovalent interactions listed in Table 2. The low magnitude of the electron density (0.005–0.024 a.u.), positive values of the Laplacian (0.018–0.097 a.u.), and close to zero positive energy density (0.001–0.003 a.u.) in these BCPs are typical for noncovalent interactions [91]. We have defined energies for these contacts according to the correlations proposed by Espinosa et al. [84] and Vener et al. [85], and one can state that the strengths of these supramolecular contacts vary from 0.6 to 5.7 kcal/mol. The balance between the Lagrangian kinetic energy $G(\mathbf{r})$ and potential energy density $V(\mathbf{r})$ at the BCPs reveals the nature of these interactions; if the ratio $-G(\mathbf{r})/V(\mathbf{r}) > 1$ is satisfied, then the nature of appropriate interaction is purely noncovalent; in case the $-G(\mathbf{r})/V(\mathbf{r}) < 1$, some covalent component takes place [92]. Based on this criterion, one can state that a covalent contribution is absent in all supramolecular contacts listed in Table 2. The negligible values of the Wiberg bond indices for these supramolecular contacts additionally confirm their electrostatic nature, and analysis of the basins of total electron density (also known as QTAIM basins) reveals that delocalization indices are also negligible for all noncovalent interactions listed in Table 1.

Table 2. Values of the density of all electrons— $\rho(\mathbf{r})$, Laplacian of electron density— $\nabla^2\rho(\mathbf{r})$, energy density— H_b , potential energy density— $V(\mathbf{r})$, Lagrangian kinetic energy— $G(\mathbf{r})$ (a.u.) at the bond critical points (3, −1), corresponding to different noncovalent interactions in $(NVP)_4 \cdot (1,4-FIB)_3$ and $(NVP)_3 \cdot (1,3-DIB)_3$, bond lengths— l (Å), as well as energies for these contacts E_{int} (kcal/mol), defined by two approaches, appropriate Wiberg bond indices (WI), and delocalization indices (DI).

Contact	$\rho(\mathbf{r})$	$\nabla^2\rho(\mathbf{r})$	H_b	$V(\mathbf{r})$	$G(\mathbf{r})$	E_{int}^1	E_{int}^2	l	WI	DI
$(NVP)_4 \cdot (1,4-FIB)_3$										
I1S...N1	0.019	0.060	0.001	−0.014	0.014	4.4	3.8	2.988	0.04	0.00
I2S...N4	0.019	0.062	0.001	−0.014	0.015	4.4	4.0	2.973	0.04	0.01
H3...O1	0.024	0.097	0.003	−0.017	0.021	5.3	5.7	1.980	0.02	0.00
H9...O1	0.005	0.020	0.001	−0.003	0.004	0.9	1.1	2.702	0.00	0.00
H2...N4	0.008	0.030	0.001	−0.004	0.006	1.3	1.6	2.601	0.00	0.00
H15B...F3S	0.005	0.026	0.001	−0.004	0.005	1.3	1.3	2.597	0.00	0.00
H12B...F4S	0.006	0.032	0.002	−0.005	0.006	1.6	1.6	2.461	0.00	0.00
H10...F1S	0.007	0.034	0.002	−0.005	0.007	1.6	1.9	2.500	0.00	0.00
H13...I1S	0.006	0.026	0.002	−0.003	0.005	0.9	1.3	3.145	0.00	0.00
H13...I2S	0.010	0.033	0.001	−0.006	0.007	1.9	1.9	2.931	0.01	0.00
C9...C11	0.007	0.022	0.001	−0.003	0.004	0.9	1.1	3.237	0.00	0.00
C2S...C2S	0.006	0.019	0.001	−0.002	0.004	0.6	1.1	3.364	0.00	0.00
C2...C4S	0.006	0.018	0.001	−0.002	0.004	0.6	1.1	3.372	0.00	0.00
$(NVP)_3 \cdot (1,3-DIB)_3$										
I1S...N1	0.012	0.043	0.001	−0.008	0.009	2.5	2.4	3.231	0.02	0.00
H3...O1	0.020	0.086	0.003	−0.015	0.018	4.7	4.8	2.035	0.01	0.01
H12A...O1	0.007	0.033	0.002	−0.004	0.006	1.3	1.6	2.585	0.00	0.00
H2...N4	0.007	0.031	0.002	−0.004	0.006	1.3	1.6	2.666	0.00	0.00
H6S...I2S	0.005	0.020	0.001	−0.003	0.004	0.9	1.1	3.172	0.00	0.00
I2S...I2S	0.014	0.043	0.001	−0.010	0.010	3.1	2.7	3.562	0.04	0.00

$$^1 E_{int} = -V(\mathbf{r})/2 \text{ [84]}. \quad ^2 E_{int} = 0.429G(\mathbf{r}) \text{ [85]}.$$

4. Conclusions

We have identified a new opportunity for co-crystallization of an active pharmaceutical ingredient, nevirapine, with 1,2,4,5-tetrafluoro-3,6-diiodobenzene, a classical XB donor, and 1,3-diiodobenzene, which has been seldom employed as an XB donor to date. Our findings provide another solid, proof-of-principle example of successfully employing halogen bonds for the design and discovery of stable crystalline forms of important drug substances. These results also lay the ground for exploring similar opportunities for other bioactive compounds with a wider range of potential donors of halogen bonds. The distinctive features of the crystal structures obtained and characterized in detail in this work are the presence of XBs with the pyridine N atoms, an XB never observed for nevirapine before. Encouraged by these findings, we aim to continue screening for novel instances of XBs stabilizing the crystal structure of active pharmaceutical ingredients. The results of these studies will be reported in due course.

Supplementary Materials: The following are available online at <http://www.mdpi.com/2073-4352/9/2/71/s1>, Table S1: Parameters of the X–H...Y HBs in the co-crystals obtained in this work; Table S2: Crystal data and structure refinement for NVP·1,4-FIB and NVP·1,3-DIB; Table S3: Cartesian atomic coordinates of model supramolecular clusters.

Author Contributions: Conceptualization: M.A.K., A.V.S., A.S.N., M.K. & D.M.I.; Data curation: M.A.K. & D.M.I.; Formal analysis: D.M.I.; Funding acquisition: A.V.S.; Investigation: M.A.K., A.S.N. & D.M.I.; Methodology: M.A.K., A.S.N. & D.M.I.; Project administration: M.K. & D.M.I.; Supervision: A.V.S., M.K. & D.M.I.; Validation: A.S.N., M.K. & D.M.I.; Visualization: A.S.N. & D.M.I.; Writing—original draft: M.K., D.M.I. & A.S.N.; Writing—review & editing: D.M.I. & A.S.N.

Funding: This work has been supported by Russian Science Foundation (project 17-73-20185).

Conflicts of Interest: The authors declare no conflict of interest. The funders had no role in the design of the study; in the collection, analyses, or interpretation of data; in the writing of the manuscript, or in the decision to publish the results.

References

1. Jie, L.; Sohrab, R. Polymorphism and Crystallization of Active Pharmaceutical Ingredients (APIs). *Curr. Med. Chem.* **2009**, *16*, 884–905. [[CrossRef](#)]
2. Yin, S.X.; Grosso, J.A. Selecting and Controlling API Crystal Form for Pharmaceutical Development—Strategies and Processes. *Curr. Opin. Drug Discov. Dev.* **2008**, *11*, 771–777.
3. Karpinski, P.H. Polymorphism of active pharmaceutical ingredients. *Chem. Eng. Technol.* **2006**, *29*, 233–237. [[CrossRef](#)]
4. Mancera, R.L. Molecular modeling of hydration in drug design. *Curr. Opin. Drug Discov. Dev.* **2007**, *10*, 275–280.
5. Morissette, S.L.; Almarsson, Ö.; Peterson, M.L.; Remenar, J.F.; Read, M.J.; Lemmo, A.V.; Ellis, S.; Cima, M.J.; Gardner, C.R. High-throughput crystallization: Polymorphs, salts, co-crystals and solvates of pharmaceutical solids. *Adv. Drug Deliv. Rev.* **2004**, *56*, 275–300. [[CrossRef](#)] [[PubMed](#)]
6. Datta, S.; Grant, D.J.W. Crystal structures of drugs: Advances in determination, prediction and engineering. *Nat. Rev. Drug Discov.* **2004**, *3*, 42–57. [[CrossRef](#)]
7. Trask, A.V. An overview of pharmaceutical cocrystals as intellectual property. *Mol. Pharm.* **2007**, *4*, 301–309. [[CrossRef](#)]
8. Blagden, N.; de Matas, M.; Gavan, P.T.; York, P. Crystal engineering of active pharmaceutical ingredients to improve solubility and dissolution rates. *Adv. Drug Deliv. Rev.* **2007**, *59*, 617–630. [[CrossRef](#)]
9. Subramanian, S.; Zaworotko, M.J. Manifestations of noncovalent bonding in the solid state. 6. $[H_4(\text{cyclam})]^{4+}$ (cyclam=1,4,8,11-tetraazacyclotetradecane) as a template for crystal engineering of network hydrogen-bonded solids. *Can. J. Chem.* **1995**, *73*, 414–424. [[CrossRef](#)]
10. Schultheiss, N.; Newman, A. Pharmaceutical Cocrystals and Their Physicochemical Properties. *Cryst. Growth Des.* **2009**, *9*, 2950–2967. [[CrossRef](#)]
11. Trask, A.V.; Motherwell, W.D.S.; Jones, W. Pharmaceutical cocrystallization: Engineering a remedy for caffeine hydration. *Cryst. Growth Des.* **2005**, *5*, 1013–1021. [[CrossRef](#)]
12. Karki, S.; Friščić, T.; Jones, W.; Motherwell, W.D.S. Screening for pharmaceutical cocrystal hydrates via neat and liquid-assisted grinding. *Mol. Pharm.* **2007**, *4*, 347–354. [[CrossRef](#)] [[PubMed](#)]
13. Aakeröy, C.B.; Salmon, D.J. Building co-crystals with molecular sense and supramolecular sensibility. *CrystEngComm* **2005**, *7*, 439–448. [[CrossRef](#)]
14. Leyssens, T.; Tumanova, N.; Robeyns, K.; Candoni, N.; Veessler, S. Solution cocrystallization, an effective tool to explore the variety of cocrystal systems: Caffeine/dicarboxylic acid cocrystals. *CrystEngComm* **2014**, *16*, 9603–9611. [[CrossRef](#)]
15. Braga, D.; Palladino, G.; Polito, M.; Rubini, K.; Grepioni, F.; Chierotti, M.R.; Gobetto, R. Three Polymorphic Forms of the Co-Crystal 4,4'-Bipyridine/Pimelic Acid and their Structural, Thermal, and Spectroscopic Characterization. *Chem. Eur. J.* **2008**, *14*, 10149–10159. [[CrossRef](#)] [[PubMed](#)]
16. James, S.L.; Adams, C.J.; Bolm, C.; Braga, D.; Collier, P.; Friscic, T.; Grepioni, F.; Harris, K.D.M.; Hyett, G.; Jones, W.; et al. Mechanochemistry: Opportunities for new and cleaner synthesis. *Chem. Soc. Rev.* **2012**, *41*, 413–447. [[CrossRef](#)] [[PubMed](#)]
17. Friščić, T.; Jones, W. Recent Advances in Understanding the Mechanism of Cocrystal Formation via Grinding. *Cryst. Growth Des.* **2009**, *9*, 1621–1637. [[CrossRef](#)]
18. Mavračić, J.; Cinčić, D.; Kaitner, B. Halogen bonding of N-bromosuccinimide by grinding. *CrystEngComm* **2016**, *18*, 3343–3346. [[CrossRef](#)]
19. Arunan, E.; Desiraju, G.R.; Klein, R.A.; Sadlej, J.; Scheiner, S.; Alkorta, I.; Clary, D.C.; Crabtree, R.H.; Dannenberg, J.J.; Hobza, P.; et al. Definition of the hydrogen bond (IUPAC Recommendations 2011). *Pure Appl. Chem.* **2011**, *83*, 1637–1641. [[CrossRef](#)]
20. Choquesillo-Lazarte, D.; Nemeč, V.; Cinčić, D. Halogen bonded cocrystals of active pharmaceutical ingredients: Pyrazinamide, lidocaine and pentoxifylline in combination with haloperfluorinated compounds. *CrystEngComm* **2017**, *19*, 5293–5299. [[CrossRef](#)]
21. Desiraju, G.R.; Ho, P.S.; Kloo, L.; Legon, A.C.; Marquardt, R.; Metrangolo, P.; Politzer, P.; Resnati, G.; Rissanen, K. Definition of the halogen bond (IUPAC Recommendations 2013). *Pure Appl. Chem.* **2013**, *85*, 1711–1713. [[CrossRef](#)]

22. Merkens, C.; Pan, F.F.; Englert, U. 3-(4-Pyridyl)-2,4-pentanedione—A bridge between coordinative, halogen, and hydrogen bonds. *CrystEngComm* **2013**, *15*, 8153–8158. [[CrossRef](#)]
23. Cinčić, D.; Friščić, T.; Jones, W. Structural Equivalence of Br and I Halogen Bonds: A Route to Isostructural Materials with Controllable Properties. *Chem. Mat.* **2008**, *20*, 6623–6626. [[CrossRef](#)]
24. Cinčić, D.; Friščić, T.; Jones, W. A cocrystallisation-based strategy to construct isostructural solids. *New J. Chem.* **2008**, *32*, 1776–1781. [[CrossRef](#)]
25. Bushuyev, O.S.; Tan, D.; Barrett, C.J.; Friščić, T. Fluorinated azobenzenes with highly strained geometries for halogen bond-driven self-assembly in the solid state. *CrystEngComm* **2015**, *17*, 73–80. [[CrossRef](#)]
26. Cinčić, D.; Friščić, T. Synthesis of an extended halogen-bonded metal-organic structure in a one-pot mechanochemical reaction that combines covalent bonding, coordination chemistry and supramolecular synthesis. *CrystEngComm* **2014**, *16*, 10169–10172. [[CrossRef](#)]
27. Troff, R.W.; Mäkelä, T.; Topić, F.; Valkonen, A.; Raatikainen, K.; Rissanen, K. Alternative Motifs for Halogen Bonding. *Eur. J. Org. Chem.* **2013**, 1617–1637. [[CrossRef](#)]
28. Cinčić, D.; Friščić, T.; Jones, W. A stepwise mechanism for the mechanochemical synthesis of halogen-bonded cocrystal architectures. *J. Am. Chem. Soc.* **2008**, *130*, 7524–7525. [[CrossRef](#)]
29. Carletta, A.; Spinelli, F.; d'Agostino, S.; Ventura, B.; Chierotti, M.R.; Gobetto, R.; Wouters, J.; Grepioni, F. Halogen-Bond Effects on the Thermo- and Photochromic Behaviour of Anil-Based Molecular Co-crystals. *Chem. Eur. J.* **2017**, *23*, 5317–5329. [[CrossRef](#)]
30. Cavallo, G.; Metrangolo, P.; Milani, R.; Pilati, T.; Priimagi, A.; Resnati, G.; Terraneo, G. The Halogen Bond. *Chem. Rev.* **2016**, *116*, 2478–2601. [[CrossRef](#)]
31. Politzer, P.; Murray, J.S.; Clark, T. Halogen bonding: An electrostatically-driven highly directional noncovalent interaction. *Phys. Chem. Chem. Phys.* **2010**, *12*, 7748–7757. [[CrossRef](#)] [[PubMed](#)]
32. Priimagi, A.; Cavallo, G.; Metrangolo, P.; Resnati, G. The Halogen Bond in the Design of Functional Supramolecular Materials: Recent Advances. *Acc. Chem. Res.* **2013**, *46*, 2686–2695. [[CrossRef](#)] [[PubMed](#)]
33. Malinska, M.; Fokt, I.; Priebe, W.; Wozniak, K. Bromine Atom Interactions in Biologically Active Acrylamide Derivatives. *Cryst. Growth Des.* **2015**, *15*, 2632–2642. [[CrossRef](#)]
34. Aakeröy, C.B.; Welideniya, D.; Desper, J.; Moore, C. Halogen-bond driven co-crystallization of potential anti-cancer compounds: A structural study. *CrystEngComm* **2014**, *16*, 10203–10209. [[CrossRef](#)]
35. Baldrighi, M.; Bartesaghi, D.; Cavallo, G.; Chierotti, M.R.; Gobetto, R.; Metrangolo, P.; Pilati, T.; Resnati, G.; Terraneo, G. Polymorphs and co-crystals of haloprogin: An antifungal agent. *CrystEngComm* **2014**, *16*, 5897–5904. [[CrossRef](#)]
36. Baldrighi, M.; Cavallo, G.; Chierotti, M.R.; Gobetto, R.; Metrangolo, P.; Pilati, T.; Resnati, G.; Terraneo, G. Halogen Bonding and Pharmaceutical Cocrystals: The Case of a Widely Used Preservative. *Mol. Pharm.* **2013**, *10*, 1760–1772. [[CrossRef](#)] [[PubMed](#)]
37. Ivanov, D.M.; Novikov, A.S.; Ananyev, I.V.; Kirina, Y.V.; Kukushkin, V.Y. Halogen bonding between metal centers and halocarbons. *Chem. Commun.* **2016**, *52*, 5565–5568. [[CrossRef](#)]
38. Ivanov, D.M.; Novikov, A.S.; Starova, G.L.; Haukka, M.; Kukushkin, V.Y. A family of heterotetrameric clusters of chloride species and halomethanes held by two halogen and two hydrogen bonds. *CrystEngComm* **2016**, *18*, 5278–5286. [[CrossRef](#)]
39. Ivanov, D.M.; Kinzhalov, M.A.; Novikov, A.S.; Ananyev, I.V.; Romanova, A.A.; Boyarskiy, V.P.; Haukka, M.; Kukushkin, V.Y. $H_2C(X)-X \cdots X^-$ ($X = Cl, Br$) Halogen Bonding of Dihalomethanes. *Cryst. Growth Des.* **2017**, *17*, 1353–1362. [[CrossRef](#)]
40. Novikov, A.S.; Ivanov, D.M.; Avdontceva, M.S.; Kukushkin, V.Y. Diiodomethane as a halogen bond donor toward metal-bound halides. *CrystEngComm* **2017**, *19*, 2517–2525. [[CrossRef](#)]
41. Bikbaeva, Z.M.; Ivanov, D.M.; Novikov, A.S.; Ananyev, I.V.; Bokach, N.A.; Kukushkin, V.Y. Electrophilic-Nucleophilic Dualism of Nickel(II) toward Ni \cdots I Noncovalent Interactions: Semicoordination of Iodine Centers via Electron Belt and Halogen Bonding via -Hole. *Inorg. Chem.* **2017**, *56*, 13562–13578. [[CrossRef](#)] [[PubMed](#)]
42. Rozhkov, A.V.; Novikov, A.S.; Ivanov, D.M.; Bolotin, D.S.; Bokach, N.A.; Kukushkin, V.Y. Structure-Directing Weak Interactions with 1,4-Diiodotetrafluorobenzene Convert One-Dimensional Arrays of $[M^{II}(acac)_2]$ Species into Three-Dimensional Networks. *Cryst. Growth Des.* **2018**, *18*, 3626–3636. [[CrossRef](#)]

43. Kinzhalov, M.A.; Kashina, M.V.; Mikherdov, A.S.; Mozheeva, E.A.; Novikov, A.S.; Smirnov, A.S.; Ivanov, D.M.; Kryukova, M.A.; Ivanov, A.Y.; Smirnov, S.N.; et al. Dramatically Enhanced Solubility of Halide-Containing Organometallic Species in Diiodomethane: The Role of Solvent...Complex Halogen Bonding. *Angew. Chem. Int. Ed.* **2018**, *57*, 12785–12789. [[CrossRef](#)] [[PubMed](#)]
44. Baykov, S.V.; Dabranskaya, U.; Ivanov, D.M.; Novikov, A.S.; Boyarskiy, V.P. Pt/Pd and I/Br Isostructural Exchange Provides Formation of C–I...Pd, C–Br...Pt, and C–Br...Pd Metal-Involving Halogen Bonding. *Cryst. Growth Des.* **2018**, *18*, 5973–5980. [[CrossRef](#)]
45. Novikov, A.S.; Ivanov, D.M.; Bikbaeva, Z.M.; Bokach, N.A.; Kukushkin, V.Y. Noncovalent Interactions Involving Iodofluorobenzenes: The Interplay of Halogen Bonding and Weak lp(O)... π -Hole_{arene} Interactions. *Cryst. Growth Des.* **2018**, *18*, 7641–7654. [[CrossRef](#)]
46. Sapegin, A.; Krasavin, M. Efficient Suzuki-Miyaura mono-arylation of symmetrical diiodo(hetero) arenes. *Tetrahedron Lett.* **2018**, *59*, 1948–1951. [[CrossRef](#)]
47. Bartlett, J.G. The DHHS adult ART guidelines are revised. *Hopkins HIV Rep.* **2005**, *17*, 6–7. [[PubMed](#)]
48. Bardsley-Elliot, A.; Perry, C.M. Nevirapine: A review of its use in the prevention and treatment of paediatric HIV infection. *Paediatr. Drugs* **2000**, *2*, 373–407. [[CrossRef](#)]
49. Gazzard, B. British HIV Association (BHIVA) guidelines for the treatment of HIV-infected adults with antiretroviral therapy (2005). *HIV Med.* **2005**, *6*, 1–61. [[CrossRef](#)]
50. Landriscina, M.; Bagala, C.; Piscazzi, A.; Schinzari, G.; Quirino, M.; Fabiano, A.; Bianchetti, S.; Cassano, A.; Sica, G.; Barone, C. Nevirapine Restores Androgen Signaling in Hormone-Refractory Human Prostate Carcinoma Cells Both In Vitro and In Vivo. *Prostate* **2009**, *69*, 744–754. [[CrossRef](#)]
51. Landriscina, M.; Spadafora, C.; Cignarelli, M.; Barone, C. Anti-tumor activity of non-nucleosidic reverse transcriptase inhibitors. *Curr. Pharm. Des.* **2007**, *13*, 737–747. [[CrossRef](#)]
52. Stefanidis, K.; Loutradis, D.; Vassiliou, L.-V.; Anastasiadou, V.; Kiapekou, E.; Nikas, V.; Patris, G.; Vlachos, G.; Rodolakis, A.; Antsaklis, A. Nevirapine induces growth arrest and premature senescence in human cervical carcinoma cells. *Gynecol. Oncol.* **2008**, *111*, 344–349. [[CrossRef](#)] [[PubMed](#)]
53. Mui, P.W.; Jacober, S.P.; Hargrave, K.D.; Adams, J. Crystal structure of nevirapine, a nonnucleoside inhibitor of HIV-1 reverse-transcriptase, and computational alignment with a structurally diverse inhibitor. *J. Med. Chem.* **1992**, *35*, 201–202. [[CrossRef](#)]
54. Da Silva, C.C.P.; Cuffini, S.L.; Faudone, S.N.; Ayala, A.P.; Ellena, J. Low-temperature study of a new nevirapine pseudopolymorph. *Acta Crystallogr. Sect. E Struct. Rep. Online* **2008**, *64*, O292. [[CrossRef](#)] [[PubMed](#)]
55. Stieger, N.; Liebenberg, W.; Wessels, J.C.; Samsodien, H.; Caira, M.R. Channel inclusion of primary alcohols in isostructural solvates of the antiretroviral nevirapine: An X-ray and thermal analysis study. *Struct. Chem.* **2010**, *21*, 771–777. [[CrossRef](#)]
56. Caira, M.R.; Bourne, S.A.; Samsodien, H.; Engel, E.; Liebenberg, W.; Stieger, N.; Aucamp, M. Co-crystals of the antiretroviral nevirapine: Crystal structures, thermal analysis and dissolution behaviour. *CrystEngComm* **2012**, *14*, 2541–2551. [[CrossRef](#)]
57. Stieger, N.; Caira, M.R.; Liebenberg, W.; Tiedt, L.R.; Wessels, J.C.; De Villiers, M.M. Influence of the Composition of Water/Ethanol Mixtures on the Solubility and Recrystallization of Nevirapine. *Cryst. Growth Des.* **2010**, *10*, 3859–3868. [[CrossRef](#)]
58. Caira, M.R.; Stieger, N.; Liebenberg, W.; De Villiers, M.M.; Samsodien, H. Solvent inclusion by the anti-HIV drug nevirapine: X-ray structures and thermal decomposition of representative solvates. *Cryst. Growth Des.* **2008**, *8*, 17–23. [[CrossRef](#)]
59. Pereira, B.G.; Fonte-Boa, F.D.; Resende, J.; Pinheiro, C.B.; Fernandes, N.G.; Yoshida, M.I.; Vianna-Soares, C.D. Pseudopolymorphs and intrinsic dissolution of nevirapine. *Cryst. Growth Des.* **2007**, *7*, 2016–2023. [[CrossRef](#)]
60. Yang, X.T.; Yu, B.H.; Zhong, Z.; Guo, B.H.; Huang, Y.B. Nevirapine-polycaprolactone crystalline inclusion complex as a potential long-acting injectable solid form. *Int. J. Pharm.* **2018**, *543*, 121–129. [[CrossRef](#)] [[PubMed](#)]
61. Kryukova, M.A.; Sapegin, A.V.; Novikov, A.S.; Krasavin, M.; Ivanov, D.M. Noncovalent interactions observed in nevirapinium pentaiodide hydrate which include the rare I₄–I[−]...O=C halogen bonding. *Z. Kristallogr. Cryst. Mater.* **2018**, in press. [[CrossRef](#)]
62. Capucci, D.; Balestri, D.; Mazzeo, P.P.; Pelagatti, P.; Rubini, K.; Bacchi, A. Liquid Nicotine Tamed in Solid Forms by Cocrystallization. *Cryst. Growth Des.* **2017**, *17*, 4958–4964. [[CrossRef](#)]

63. Sugiyama, H.; Uekusa, H. Relationship between crystal structures and photochromic properties of N-salicylideneaminopyridine derivatives. *CrystEngComm* **2018**, *20*, 2144–2151. [[CrossRef](#)]
64. Sheldrick, G. SHELXT—Integrated space-group and crystal-structure determination. *Acta Cryst. A* **2015**, *71*, 3–8. [[CrossRef](#)] [[PubMed](#)]
65. Dolomanov, O.V.; Bourhis, L.J.; Gildea, R.J.; Howard, J.A.K.; Puschmann, H. OLEX2: A complete structure solution, refinement and analysis program. *J. Appl. Cryst.* **2009**, *42*, 339–341. [[CrossRef](#)]
66. Agilent Technologies Ltd. *CrysAlisPro*; Version 1.171.136.120 (release 127-106-2012); Agilent Technologies Ltd.: Santa Clara, CA, USA, 2012.
67. Zhao, Y.; Truhlar, D.G. The M06 suite of density functionals for main group thermochemistry, thermochemical kinetics, noncovalent interactions, excited states, and transition elements: Two new functionals and systematic testing of four M06-class functionals and 12 other functionals. *Theor. Chem. Acc.* **2008**, *120*, 215–241. [[CrossRef](#)]
68. Frisch, M.J.; Trucks, G.W.; Schlegel, H.B.; Scuseria, G.E.; Robb, M.A.; Cheeseman, J.R.; Scalmani, G.; Barone, V.; Mennucci, B.; Petersson, G.A.; et al. *Gaussian 09*, Revision D.01; Gaussian, Inc.: Wallingford, CT, USA, 2009.
69. Barros, C.L.; de Oliveira, P.J.P.; Jorge, F.E.; Canal Neto, A.; Campos, M. Gaussian basis set of double zeta quality for atoms Rb through Xe: Application in non-relativistic and relativistic calculations of atomic and molecular properties. *Mol. Phys.* **2010**, *108*, 1965–1972. [[CrossRef](#)]
70. De Berrêdo, R.C.; Jorge, F.E. All-electron double zeta basis sets for platinum: Estimating scalar relativistic effects on platinum(II) anticancer drugs. *J. Mol. Struct. THEOCHEM* **2010**, *961*, 107–112. [[CrossRef](#)]
71. Jorge, F.E.; Canal Neto, A.; Camiletti, G.G.; Machado, S.F. Contracted Gaussian basis sets for Douglas–Kroll–Hess calculations: Estimating scalar relativistic effects of some atomic and molecular properties. *J. Chem. Phys.* **2009**, *130*, 064108. [[CrossRef](#)]
72. Neto, A.C.; Jorge, F.E. All-electron double zeta basis sets for the most fifth-row atoms: Application in DFT spectroscopic constant calculations. *Chem. Phys. Lett.* **2013**, *582*, 158–162. [[CrossRef](#)]
73. Bader, R.F.W. A quantum theory of molecular structure and its applications. *Chem. Rev.* **1991**, *91*, 893–928. [[CrossRef](#)]
74. Lu, T.; Chen, F. Multiwfn: A multifunctional wavefunction analyzer. *J. Comput. Chem.* **2012**, *33*, 580–592. [[CrossRef](#)] [[PubMed](#)]
75. Glendening, E.D.; Landis, C.R.; Weinhold, F. Natural bond orbital methods. *Wiley Interdiscip. Rev. Comput. Mol. Sci.* **2012**, *2*, 1–42. [[CrossRef](#)]
76. Roper, L.C.; Prasang, C.; Kozhevnikov, V.N.; Whitwood, A.C.; Karadakov, P.B.; Bruce, D.W. Experimental and Theoretical Study of Halogen-Bonded Complexes of DMAP with Di- and Triiodofluorobenzenes. A Complex with a Very Short N⋯I Halogen Bond. *Cryst. Growth Des.* **2010**, *10*, 3710–3720. [[CrossRef](#)]
77. Eccles, K.S.; Morrison, R.E.; Sinha, A.S.; Maguire, A.R.; Lawrence, S.E. Investigating C=S⋯I Halogen Bonding for Cocrystallization with Primary Thioamides. *Cryst. Growth Des.* **2015**, *15*, 3442–3451. [[CrossRef](#)]
78. Walsh, R.B.; Padgett, C.W.; Metrangolo, P.; Resnati, G.; Hanks, T.W.; Pennington, W.T. Crystal engineering through halogen bonding: Complexes of nitrogen heterocycles with organic iodides. *Cryst. Growth Des.* **2001**, *1*, 165–175. [[CrossRef](#)]
79. Yan, D.P.; Delori, A.; Lloyd, G.O.; Friščić, T.; Day, G.M.; Jones, W.; Lu, J.; Wei, M.; Evans, D.G.; Duan, X. A Cocrystal Strategy to Tune the Luminescent Properties of Stilbene-Type Organic Solid-State Materials. *Angew. Chem. Int. Ed.* **2011**, *50*, 12483–12486. [[CrossRef](#)] [[PubMed](#)]
80. Ravat, P.; SeethaLekshmi, S.; Biswas, S.N.; Nandy, P.; Varughese, S. Equivalence of Ethylene and Azo-Bridges in the Modular Design of Molecular Complexes: Role of Weak Interactions. *Cryst. Growth Des.* **2015**, *15*, 2389–2401. [[CrossRef](#)]
81. Cerreia Vioglio, P.; Catalano, L.; Vasylyeva, V.; Nervi, C.; Chierotti, M.R.; Resnati, G.; Gobetto, R.; Metrangolo, P. Natural Abundance ¹⁵N and ¹³C Solid-State NMR Chemical Shifts: High Sensitivity Probes of the Halogen Bond Geometry. *Chem. Eur. J.* **2016**, *22*, 16817–16826. [[CrossRef](#)]
82. Ji, B.M.; Wang, W.Z.; Deng, D.S.; Zhang, Y.; Cao, L.; Zhou, L.; Ruan, C.S.; Li, T.S. Structural competition between $\pi\cdots\pi$ interactions and halogen bonds: A crystallographic study. *CrystEngComm* **2013**, *15*, 769–774. [[CrossRef](#)]
83. Bondi, A. Van der Waals volumes and radii. *J. Phys. Chem.* **1964**, *68*, 441–451. [[CrossRef](#)]
84. Espinosa, E.; Molins, E.; Lecomte, C. Hydrogen bond strengths revealed by topological analyses of experimentally observed electron densities. *Chem. Phys. Lett.* **1998**, *285*, 170–173. [[CrossRef](#)]

85. Vener, M.V.; Egorova, A.N.; Churakov, A.V.; Tsirelson, V.G. Intermolecular hydrogen bond energies in crystals evaluated using electron density properties: DFT computations with periodic boundary conditions. *J. Comput. Chem.* **2012**, *33*, 2303–2309. [[CrossRef](#)] [[PubMed](#)]
86. Adonin, S.A.; Udalova, L.I.; Abramov, P.A.; Novikov, A.S.; Yushina, I.V.; Korolkov, I.V.; Semitut, E.Y.; Derzhavskaya, T.A.; Stevenson, K.J.; Troshin, P.A.; et al. A Novel Family of Polyiodo-Bromoantimonate(III) Complexes: Cation-Driven Self-Assembly of Photoconductive Metal-Polyhalide Frameworks. *Chem. Eur. J.* **2018**, *24*, 14707–14711. [[CrossRef](#)] [[PubMed](#)]
87. Mikherdov, A.S.; Kinzhalov, M.A.; Novikov, A.S.; Boyarskiy, V.P.; Boyarskaya, I.A.; Avdontceva, M.S.; Kukushkin, V.Y. Ligation-Enhanced π -Hole $\cdots\pi$ Interactions Involving Isocyanides: Effect of -Hole \cdots Noncovalent Bonding on Conformational Stabilization of Acyclic Diaminocarbene Ligands. *Inorg. Chem.* **2018**, *57*, 6722–6733. [[CrossRef](#)] [[PubMed](#)]
88. Adonin, S.A.; Bondarenko, M.A.; Abramov, P.A.; Novikov, A.S.; Plyusnin, P.E.; Sokolov, M.N.; Fedin, V.P. Bromo- and Polybromoantimonates(V): Structural and Theoretical Studies of Hybrid Halogen-Rich Halometalate Frameworks. *Chem. Eur. J.* **2018**, *24*, 10165–10170. [[CrossRef](#)] [[PubMed](#)]
89. Mikherdov, A.S.; Novikov, A.S.; Kinzhalov, M.A.; Boyarskiy, V.P.; Starova, G.L.; Ivanov, A.Y.; Kukushkin, V.Y. Halides Held by Bifurcated Chalcogen-Hydrogen Bonds. Effect of $\mu_{(S,N-H)}$ -Cl-(S,Cl-N-H) Contacts on Dimerization of Cl(carbene)Pd^{II} Species. *Inorg. Chem.* **2018**, *57*, 3420–3433. [[CrossRef](#)]
90. Johnson, E.R.; Keinan, S.; Mori-Sánchez, P.; Contreras-García, J.; Cohen, A.J.; Yang, W. Revealing Noncovalent Interactions. *J. Am. Chem. Soc.* **2010**, *132*, 6498–6506. [[CrossRef](#)]
91. Grabowski, S.J. Noncovalent interactions—QTAIM and NBO analysis. *J. Mol. Model.* **2013**, *19*, 4713–4721. [[CrossRef](#)]
92. Espinosa, E.; Alkorta, I.; Elguero, J.; Molins, E. From weak to strong interactions: A comprehensive analysis of the topological and energetic properties of the electron density distribution involving X–H \cdots F–Y systems. *J. Chem. Phys.* **2002**, *117*, 5529–5542. [[CrossRef](#)]



© 2019 by the authors. Licensee MDPI, Basel, Switzerland. This article is an open access article distributed under the terms and conditions of the Creative Commons Attribution (CC BY) license (<http://creativecommons.org/licenses/by/4.0/>).